Journal of Membrane Science 496 (2015) 1–12

Contents lists available at ScienceDirect

Journal of Membrane Science

journal homepage: www.elsevier.com/locate/memsci

CO_2 capture using a superhydrophobic ceramic membrane contactor

Xinhai Yu [a,b,*], Lin An [a], Jie Yang [c], Shan-Tung Tu [a], Jinyue Yan [d,e]

[a] Key Laboratory of Pressure Systems and Safety (MOE), School of Mechanical Engineering, East China University of Science and Technology, Shanghai, China
[b] State Key Laboratory of Bioreactor Engineering, East China University of Science and Technology, Shanghai, China
[c] School of Energy and Power Engineering, University of Shanghai for Science and Technology, Shanghai, China
[d] School of Business Society and Technology, Mälardalen University, Västerås, Sweden
[e] School of Chemical Science and Engineering, Royal Institute of Technology, Stockholm, Sweden

ARTICLE INFO

Article history:
Received 3 February 2015
Received in revised form
12 May 2015
Accepted 30 August 2015
Available online 2 September 2015

Keywords:
Superhydrophobic
Ceramic
Membrane contactor
CO_2 capture
Wetting

ABSTRACT

The wetting and fouling of a membrane contactor deteriorated performance of the membrane gas absorption system for CO_2 post-combustion capture in coal-fired power plants. To solve these problems, in this study, a superhydrophobic ceramic (SC) membrane contactor was fabricated from an alumina tube with a ZrO_2 layer by means of grafting with fluoroalkylsilane (FAS) in a triethoxy-1H,1H,2H,2H-tridecafluoro-n-octylsilane solution. The performances of the SC membrane contactor and polypropylene (PP) hollow fiber membrane contactor were compared through experiments conducted in a CO_2 absorption experimental system using a monoethanolamine (MEA) aqueous solution. Although the membrane fabrication cost per effective membrane area (*CPA*) of the SC membrane is 12.5 times that of the PP hollow fiber membrane, the SC membrane fabrication cost per absorbed CO_2 flux (*CPC*) was lower than that of the PP membrane. For the SC membrane, the detrimental effect of wetting can be alleviated by periodic drying to ensure a high CO_2 removal efficiency ($>90\%$). Drying does not work for the PP membrane because the swelling of the PP fibers is irreversible. The SC membrane contactor exhibited a better anti-fouling ability than the PP membrane contactor because the superhydrophobic surface can self-clean. To ensure a continuous, high-efficiency CO_2 removal, a method was proposed in which two-hollow fiber SC membrane contactors operate alternately with the addition of periodic drying. The SC hollow fiber membrane contactor shows great potential in real industrial CO_2 post-combustion capture because of its good anti-wetting and anti-fouling features.

1. Introduction

Carbon capture and storage (CCS) has been recognized as one approach for mitigating CO_2 emissions, especially from large fossil fuel combustion units, such as those used for electric power generation and other industrial processes. The capture and compression of CO_2 from power plant flue gas account for over 75% of the total cost of carbon capture and storage (CCS) [1]. To achieve mid- to long-term CO_2 reduction targets, the cost-effective methods to capture CO_2 from fossil-fuel power plants and the options for CO_2 subsequent sequestration need to be evaluated given the world's growing demand for energy. At present, a wide variety of technological options have been proposed to capture CO_2 emitted during the combustion of fossil fuels, such as chemical and physical absorption, solid adsorption, cryogenic distillation, and membrane techniques [2–4].

The membrane gas-absorption process is a hybrid technology that combines the advantages of chemical (high selectivity) and membrane (modularity and compact structure) absorption. CO_2 separated from flue gas is diffused through membrane, and then recovered by a liquid absorbent. This process exhibits a higher removal rate than a gas-separation membrane because of the continuous high driving force. Compared to conventional absorption devices such as packed towers and bubble columns, the membrane contactor has the features of operational flexibility, independent gas and liquid flow, a high surface-area-to-volume ratio, a compact size, easy scale-up, and modularity [5]. Because of its excellent mass-transfer properties, membrane gas-absorption technology has been identified as a technically viable option by the International Energy Agency's working group on CO_2 capture and has been considered a promising alternative to conventional and potential large-scale application technologies for CO_2 removal [6].

However, a disadvantage of the membrane contactors is the presence of an additional diffusion resistance (through the membrane pores), which becomes significant when the membrane pores are wetted by liquid absorbents, thus, leading to the deterioration of the CO_2 absorption flux in long-term operation. The

* Corresponding author at: Key Laboratory of Pressure Systems and Safety (MOE), School of Mechanical Engineering, East China University of Science and Technology, Shanghai, China.
E-mail address: yxhh@ecust.edu.cn (X. Yu).

http://dx.doi.org/10.1016/j.memsci.2015.08.062
0376-7388/

non-wetting mode can obtain the minimal diffusion resistance in the membrane pores [7,8]. The operational mode depends in part on the membrane materials. At present, most of the commercially available hollow fiber membranes are made from polymeric materials such as polypropylene (PP), polyvinylidene fluoride, polytetrafluoroethylene, polysulfone, polyether sulfone (PES), polyimide, polyethylene (PE) [9–14], most of which suffer from chemical and thermal stresses due to contact with absorbents, leading to membrane swelling and morphological changes [15–17]. These changes can increase the overall mass transfer resistance and degrade the performance of the membranes. There are a large number of reports on membrane wetting. Zhang et al. [18] found that that for a PP module, the CO_2 flux dropped severely after two days of operation and finally stabilized on the 4th day, while for a polyvinylidene fluoride (PVDF) module the operation failed due to the appearance of diethanol amine (DEA) droplets in the gas phase after initial several times of running. Keshavarz et al. investigated the effect of the membrane-wetting fraction on the chemical reactions in the wetted pores; the theoretical results showed that the absorption flux could significantly decrease by membrane wetting, even in very low fractions [19]. Mavroudi et al. [20] studied membrane wetting in gas-absorption membrane systems and found that membrane mass-transfer resistance accounted for 20–50% of the total resistance in the case of liquid-filled membrane pores. Lv et al. experimentally investigated the interaction between absorbents and membranes and characterized the effect of membrane wetting on membrane properties [21]. Their experimental results confirmed that the absorbent molecules diffuse into the PP polymers during the exposure process, resulting in the swelling of the membranes. In accordance with the Laplace–Young equation, improving membrane surface hydrophobicity may be effective in overcoming wetting. To this end, Lv et al. [22] modified the PP membrane fiber by depositing a rough layer on the surface to improve its hydrophobicity. The contact angle increased dramatically from 122° to 158° by the modification, thereby obtaining a superhydrophobic membrane surface. The long-term system operation results indicate that the modification treatment effectively enhanced the membrane stability. However, additional mass-transfer resistance was introduced by the surface coating. Therefore, more efforts are needed to solve the problem of membrane wetting.

Compared with the polymeric membranes, ceramic membranes show better structural, thermal, physical and chemical stability and have been widely applied in the separation and purification processes [23]. Most ceramic membranes are made from metal oxides, such as alumina, zirconia, silica and so on, which are hydrophilic in nature because of the presence of hydroxyl (OH^-) groups on the surface [24]. This surface property prevents them from being directly used in membrane gas-absorption process. However, the ceramic membranes with hydrophobic surface could be prepared by surface modification [25]. Fang et al. [26] reported the development of hydrophobic porous alumina ceramic hollow fiber membranes via grafting with fluoroalkylsilane (FAS) for water desalination based on the membrane distillation process. Koonaphapdeelert and Li prepared alumina hollow fiber membranes and modified them to be hydrophobic by grafting them with 0.01 mol/l of FAS solution. The grafted ceramic hollow fiber membranes were thermally stable up to 250 °C and showed solvent stability with hexane [27]. Hydrophobic ceramic hollow fiber membrane contactors were applied to strip CO_2 from an amine solution for the first time by Koonaphapdeelert et al. [28]. However, to date there has been no report on the use of hydrophobic ceramic hollow fiber membranes for CO_2 absorption.

In addition, fouling is one of the major problems in the industrial application of porous membranes. Fortunately, in the gas–liquid contactor applications, the contactors are less sensitive to fouling because there is no convection flow through the membrane pores. However, in industrial applications such as coal-fired power plants, gas and liquid streams with suspended particles can cause plugging due to the small membrane contactor diameter. So far there has been no report on the fouling of membrane contactors for CO_2 capture.

In this study, a superhydrophobic ceramic (SC) membrane contactor starting from an alumina tube with a ZrO_2 layer was fabricated by means of grafting with FAS of triethoxy-1H,1H,2H,2H-tridecafluoro-n-octylsilane solution for CO_2 absorption to address the problems of membrane wetting and fouling. The SC membrane contactor was characterized by various characterization methods, including contact angle measurement, gas permeation method, pure water permeation method, scanning electron microscopy (SEM), X-ray photoemission and spectroscopy (XPS). The performances of SC membrane contactors and PP hollow fiber membrane contactors were compared through experiments conducted in a CO_2 absorption experimental system using monoethanolamine (MEA) aqueous solution. The anti-fouling of the SC membrane contactor was investigated by continuous operation in a coal-fired power plant.

2. Experimental

2.1. Membrane modification

For the process of surface hydrophobic modification, the ceramic membrane tubes (Jangsu Jiuwu Hi-tech Co., Ltd.) were firstly cleaned by ultrasonication in ethanol and deionized water. The ceramic membrane was fabricated by coating a ZrO_2 membrane layer on the interior surface of a highly permeable porous alumina support. Then, the ceramic membrane tubes were soaked in a mixture of ethanol and deionized water (2:1; volume) for 24 h and dried in an electrically heated drying oven at 60 °C for 24 h. The dried ceramic membrane tubes were immersed into the solution of 2 wt% FAS of triethoxy-1H,1H,2H,2H-tridecafluoro-n-octylsilane (Shanghai Hansi Chemical Co., Ltd.) and 98 wt% ethanol at room temperature for 24 h. After the immersion, the ceramic membrane tubes were rinsed with ethanol and deionized water to get rid of the unreacted FAS residue. The ceramic membrane tubes were subsequently dried at 100 °C for 24 h.

2.2. Membrane characterization

The pore size distributions of the ceramic membranes were measured by the bubble point method reported by Jakobs et al. [29]. SEM images of the SC membrane contactor were obtained using a JEOL JSM 6360M scanning electron microscope (SEM) equipped with an EDAX FALCON energy dispersive X-ray spectrometry (EDS) unit. SEM images of the PP hollow fibers were observed under a JEOL JSM-7401FFE-SEM. The accelerating voltage used was 5 kV. The images of the PP fiber surfaces were captured by a video recorder attached to a Macintosh computer system. The images were digitized and analyzed using Image-Pro-Plus Version 5.0 software.

The contact angle was measured using an OCA20 Micro Tensiometer (Dataphysics Corp., Germany) to evaluate the ceramic membrane's hydrophobicity. A droplet of distilled water was placed on the membrane surface using a 0.40 ml syringe. The contact angles were calculated from a digital video image of the droplet on the membrane surface. An image-processing program was used to estimate the contact angle using the drop's height and width. To minimize experimental errors, the contact angles were obtained by averaging five measurements.

XPS experiments were carried out using a Thermo ESCALAB

250 spectrometer (Perkin Elmer). A monochromatic Al Kα radiation source ($h\nu$=1486.6 eV) was used with a spot size of 300 μm. The binding energies (BEs) were calibrated using containment carbon (C1s=284.6 eV).

Gas permeation and liquid permeation of the un-grafted ceramic membranes and SC membrane were measured. Nitrogen was used as the test gas for the gas permeation measurement. The ceramic membrane tube was fixed on the base of a male connector and the one end was sealed off with epoxy resin. Then, the ceramic membrane tube was covered by a refined cylinder. Nitrogen was fed into the cylinder at different pressures, and the gas permeation through the tube was measured by a soap bubble flow meter. The permeation values of pure water and 5 wt% MEA aqueous solution were tested using a similar device to that for gas permeation, in which pure water was fed into the cylinder by pressurized nitrogen, and the weight of the permeated liquid was determined using an electronic balance (CPA225D, Sartorius Scientific Instruments (Beijing) Co. Ltd., China).

2.3. CO_2 absorption

Fig. 1 shows the schematic diagram of CO_2 absorption using a SC or PP membrane contactor. The PP membrane contactor (obtained from the 718th Institute of China Shipbuilding Industry Corporation) was used as the absorber. The specifications of the SC and PP membrane contactors are listed in Table 1. A gas mixture containing CO_2 and N_2 with a volume ratio of 12.5:87.5 was used, which is in the composition range of flue gas from coal-fired power station. The MEA of 99.5% analytical grade (Shanghai Bangcheng Chemical Co., Ltd., China) was dissolved in deionized water to prepare the aqueous MEA solution. The gas and liquid flowed countercurrent through the module (the absorbent passed through the lumen side, and the gas flowed countercurrent through the shell side of the hollow fibers).

In the experiments, CO_2 and N_2 were introduced into the system from compressed gas cylinders and the flow rate was adjusted by two mass flow controllers (MFC D07, Sevenstar Electronics Co., Ltd.), which precisely controlled the gas flow rate. Then, CO_2 and N_2 flowed into a static mixer where they were mixed uniformly. After flowing through a press gauge (Ashcroft), the mixed gas entered membrane module from the shell side. A throttling value (LA-H8L, Yueqing Yade Pneumatic Co., Ltd.) was connected with the gas outlet to adjust the gas pressure. The temperature of the gas was kept at 293 K. The inlet and outlet gas compositions were analyzed on-line by a 9790 III gas chromatograph (FuLi Analytical Instrument Co., Ltd.) using a thermal conductivity detector (TCD). The absorbent solution was stored in a container that was immersed into a water batch. The absorbent solution temperature was controlled by adjusting the temperature of the water batch. Hereinafter, the temperature of absorbent solution was 293 K except as otherwise noted. A plunger metering pump (2PB00C, Beijing Satellite Manufacturing Factory) was used to pump the absorbent solution into the lumen side of the membranes from the absorbent solution container with a controlled and constant liquid flow rate. A press gauge (Shanghai Ronghua Instrument Co., Ltd.) at the inlet of the lumen side was used to measure the absorbent solution pressure. A throttling value (LA-H8L, Yueqing Yade Pneumatic Co., Ltd.) at the outlet of the absorbent solution adjusted the absorbent pressure. The absorbent concentrations at the inlet and outlet were measured by a chemical titrimetric method. In what follows, the two throttling values at the outlets of the gas and absorbent solution were fully opened and the the pressures of the gas and absorbent solution roughly equaled to atmosphere pressure unless otherwise specified. All of the data were collected in a steady state.

3. Results and discussion

3.1. Membrane characterization

The water contact angles (see Fig. 2) of the ceramic membranes un-grafted and grafted by FAS were measured. The contact angle of the un-grafted membranes could not be obtained because the droplet of deionized water was quickly sucked into the porous membrane. After grafting by FAS, the ceramic membrane achieved a contact angle of 153°, revealing that the membrane surface was modified from hydrophilicity to superhydrophobicity. The superhydrophobicity indicated that most of the hydroxyl groups on the membrane surface reacted with FAS because the hydrophilicity is heavily dependent on the density of hydroxyl groups [30].

Fig. 3 shows N_2 permeance as a function of the trans SC membrane pressure. The N_2 permeance of the SC membrane was approximately 7.90×10^{-3} mol m^{-2} s^{-1} Pa^{-1}, which was only slightly lower than that of 8.9×10^{-3} mol m^{-2} s^{-1} Pa^{-1} for the un-grafted ceramic membrane; this result suggests that the

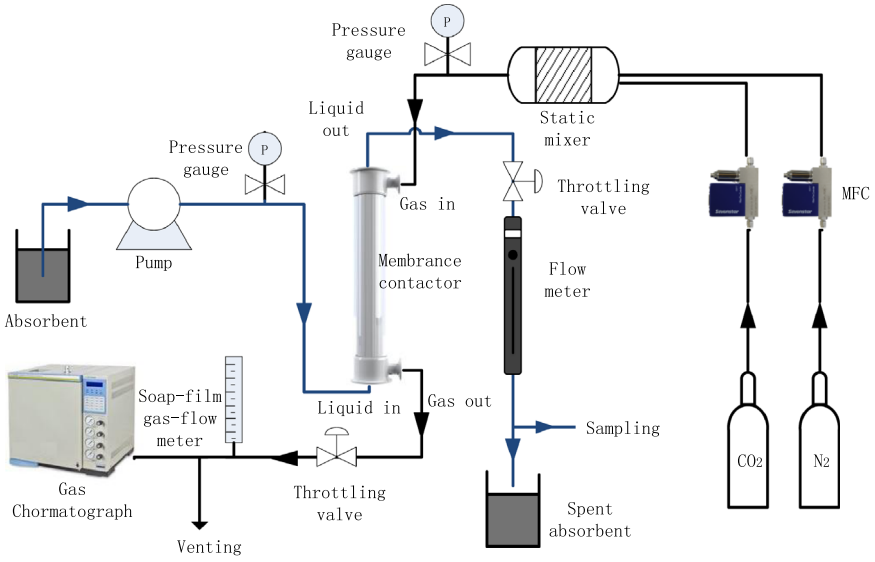

Fig. 1. Schematic diagram of experimental setup.

Table 1
The specifications of membrane modules.

Module parameters	Module 1	Module 2	Unit
Membrane material	Support layer of alumina and membrane layer of ZrO_2 grafted by FAS	PP	
Module inner diameter	30	42	mm
Module length	380	440	mm
Membrane tube inner diameter	8	0.26	mm
Membrane tube outer diameter	12	0.38	mm
Membrane tube length	360	440	mm
Number of membrane tube	1	2000	dimensionless
Membrane tube porosity	0.38	0.45	dimensionless
Pore size	0.20	0.15	μm
Effective membrane area	0.00344	0.323	m^2

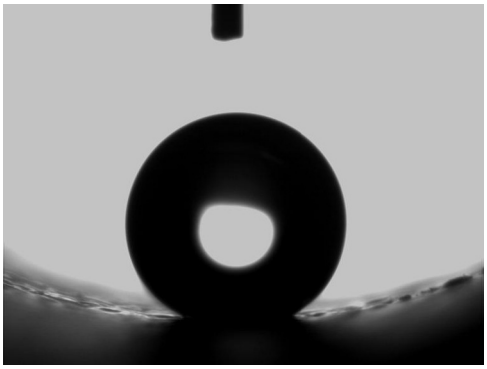

Fig. 2. Image of a water drop on the SC membrane surface.

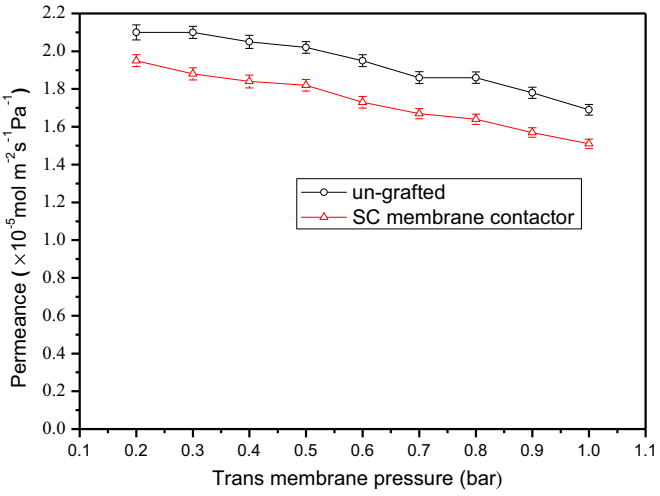

Fig. 3. N_2 permeance as function of trans-membrane pressure of un-grafted and SC membrane contactors.

grafted FAS reduces the pore sizes of the membrane slightly. However, the FAS grafting led to a drastic decrease in the permeance of clean water because of the increased surface hydrophobicity. As shown in Fig. 4, the un-grafted ceramic membrane allowed liquid water to pass through at a fast rate of 1.94 $m^3\ m^{-2}\ h^{-1}\ bar^{-1}$, whereas the SC membrane completely blocked water and 5% MEA aqueous solution at trans-membrane pressures less than 6.5 and 5.5 bar, respectively. Only at a pressure above those values did water and 5% MEA aqueous solution start to permeate through the membrane. These critical entry pressures agree well with the values calculated by the Laplace's equation [31].

Fig. 5a and b show the micrographs of the outer surface of the un-grafted ceramic membrane and the SC membrane, respectively. There was no clear indication of the presence of a FAS film. The FAS

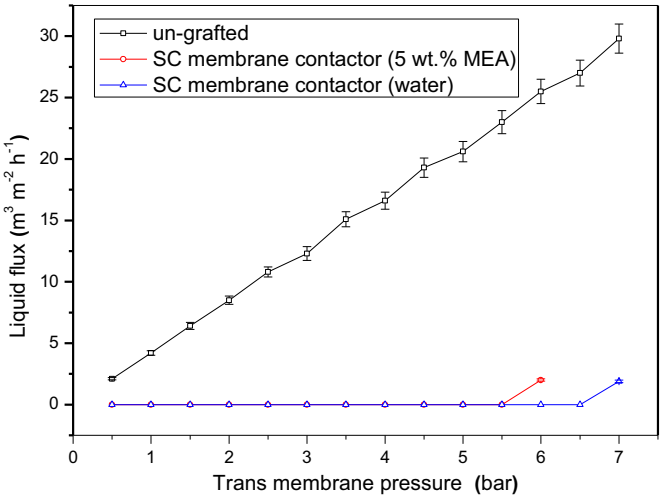

Fig. 4. Liquid flux as function of trans-membrane pressure of un-grafted and SC membrane contactors using water and 5 wt% MEA aqueous solution at 298 K.

molecules were only bonded to the surface but did not polymerize to form a thick layer to be seen because the number of hydroxyl groups on the surface of sintered ZrO_2 membrane was limited. As a result, the overall structures and the surface porosity of these two membranes hardly changed. This might be the reason why the gas permeance, as shown in Fig. 3, slightly decreased after the FAS grafting.

The presence of FAS on the SC membrane was confirmed by XPS analysis. Fig. 6 shows the XPS spectra of the un-grafted ceramic membrane and the SC membrane, respectively. The characteristic peaks of zirconium, oxygen and carbon atoms were observed in the two samples because those species are the main compositions of the ceramic membranes in our case. Compared to the un-grafted membrane, an obvious F1s peak at 688.6 eV and a weak –Si–O– peak at 102.6 eV appeared for the SC membrane, indicating the presence of grafted fluoroalkylsilane on the membrane surface.

3.2. *Performances of SC membrane in CO_2 absorption*

In this study, removal efficiency and mass transfer rate of CO_2 were used to evaluate the separation properties of membranes, which can be calculated by Eqs. (1) and (2), respectively [32]:

$$\eta = \frac{Q_{g,\,in} \times C_{g,\,in} - Q_{g,\,out} \times C_{g,\,out}}{Q_{g,\,in} \times C_{g,\,in}} \tag{1}$$

$$J = \frac{\left(Q_{g,\,in} \times C_{g,\,in} - Q_{g,\,out} \times C_{g,\,out}\right) \times 273.15}{0.0224 \times T_g \times S} \tag{2}$$

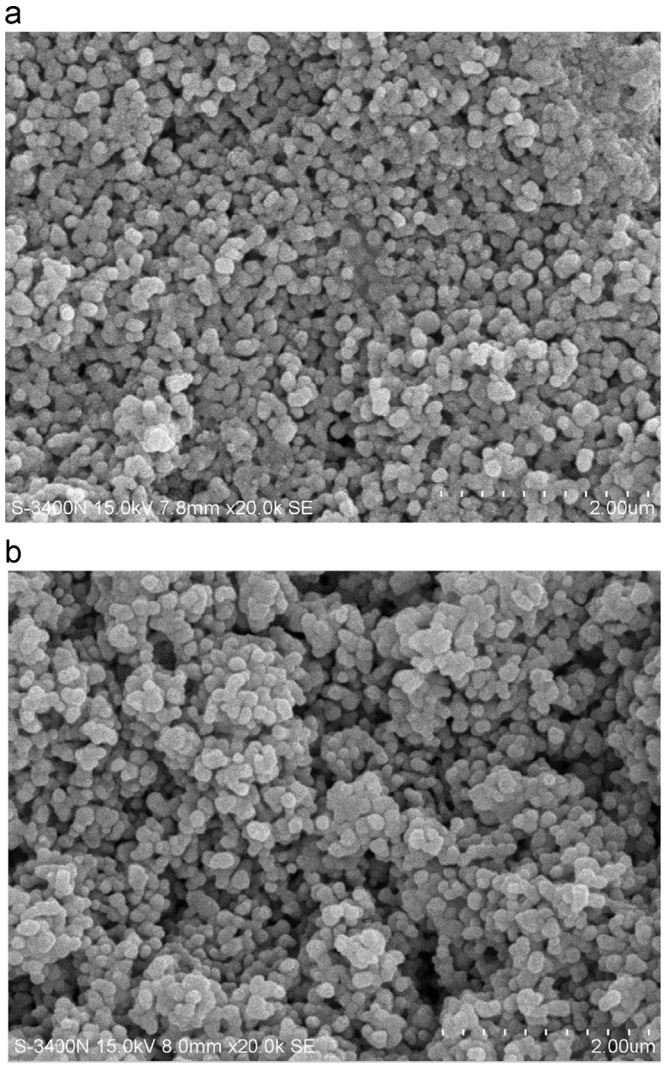

Fig. 5. SEM image of ceramic membrane surface: (a) un-grafted and (b) SC.

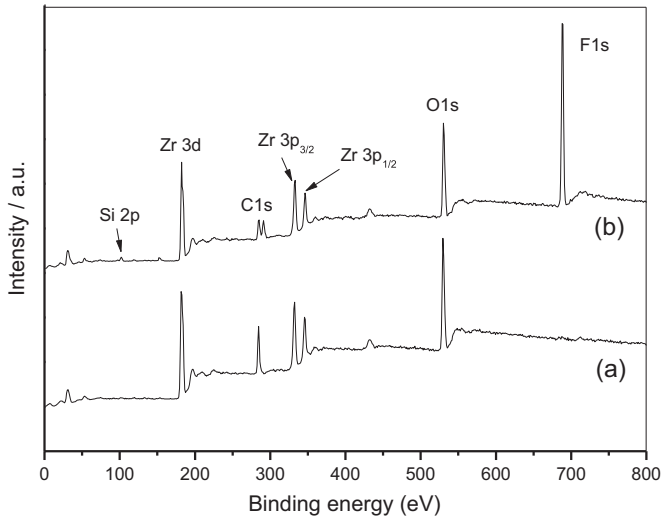

Fig. 6. XPS spectra of ceramic membrane surface: (a) un-grafted and (b) SC.

The average of five measurements were used for the calculations in this study and all of the data were obtained under steady conditions within 2 h when the concentration of CO_2 was constant in the gas stream at the outlet of membrane contactor.

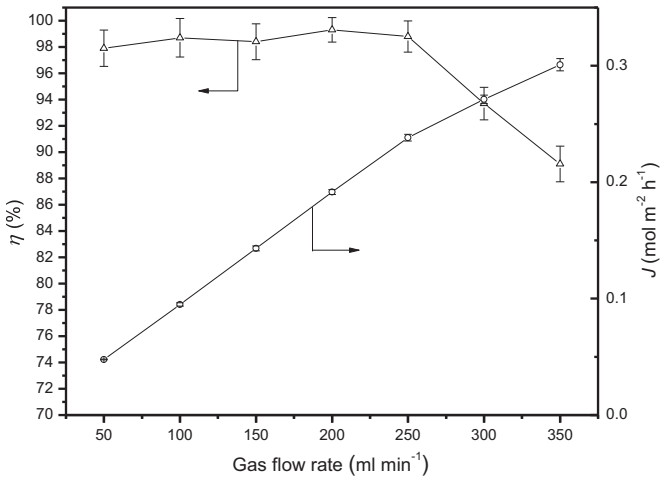

Fig. 7. Effect of gas flow rate on CO_2 absorption for PP hollow fiber membrane (absorbent flow rate of 50 ml min^{-1}; gas and absorbent temperatures of 293 K; absorbent of 5 wt% MEA aqueous solution; CO_2 concentration in feed gas of 12.5%).

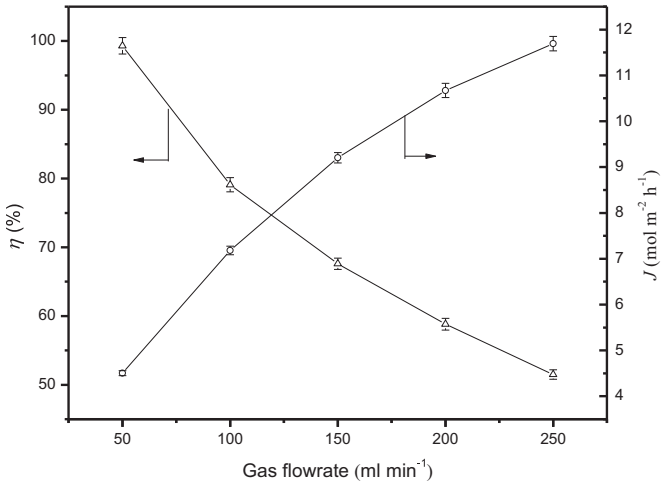

Fig. 8. Effect of gas flow rate on CO_2 absorption for SC membrane (absorbent flow rate of 10 ml min^{-1}; gas and absorbent temperatures of 293 K; absorbent of 5 wt% MEA aqueous solution; CO_2 concentration in feed gas of 12.5%).

Figs. 7 and 8 show the effects of gas flow rate. For the PP membrane, the CO_2 removal efficiency of η kept stable when the gas flow rate increased form 50 to 250 ml min^{-1} and then decreased quickly. The mass transfer rate of J increased linearly with the rise of the gas flow rate from 50 to 350 ml min^{-1}. The tendencies for the SC membrane are similar except that the CO_2 removal efficiency dropped continuously and remarkably with the gas flow rate from 50 to 250 ml min^{-1}.

For a membrane contactor, the feed gas and absorbent liquid flow on the opposite sides of the membrane. CO_2 contained in the gas phase passes through the membrane, whereas absorption occurs on the liquid side. The mass-transfer process consists of three consecutive steps: (i) diffusion from bulk gas phase to the outer surface of the membrane; (ii) diffusion through membrane pores; and (iii) dissolution into the absorption liquid and liquid-phase diffusion/chemical reaction. Consequently, for a hydrophobic hollow fiber membrane with gas-filled pores and liquid absorbent in the lumen side, the overall liquid phase mass transfer coefficient (k_o) can then be expressed by a resistance in series model [23], as described in Eq. (3)

$$k_o^{-1} = H\left(k_g \cdot \frac{d_o}{d_i}\right)^{-1} + H\left(k_m \cdot \frac{d_{lm}}{d_i}\right)^{-1} + (E \cdot k_l)^{-1} \quad (3)$$

For gas absorption, the resistance to gas diffusion from the bulk gas to the membrane external surface can be ignored compared to other resistances [33]. Accordingly, the increase of the gas flow rate cannot obviously enhance the CO_2 mass transfer rate. On the other hand, the membrane resistance depends on the membrane operation mode, i.e., non-wetted, wetted or partially wetted mode. The high gas flow rate raised the gas pressure outside the membrane fiber, thus pushing amount of water out from the fiber pores and alleviating the membrane wetting. This gave rise to the increase of CO_2 mass transfer rate as shown in Figs. 7 and 8 because wetting increases the membrane mass transfer resistance rapidly and significantly [34]. Despite the increase of the CO_2 mass transfer rate with the gas flow rate, the CO_2 residence time declined, which is unfavorable for CO_2 absorption. The whole two effects resulted in the decrease of the CO_2 removal efficiency, indicating that the unfavorable effect of short residence time overwhelmed the favorable effect of high CO_2 mass transfer rate in this case.

The effects of MEA concentration on the CO_2 absorption of the SC membrane were illustrated in Fig. 9. When the MEA concentration rose from 0 to 5 wt%, the CO_2 removal efficiency and CO_2 mass transfer rate increased from 6.12% to 99.8% and from 0.122 to 1.96 mol m^{-2} h^{-1}, respectively. Therefore, the mass transfer can be enhanced in the presence of a chemical reaction. The enhancement factor E describes the effect of a chemical reaction on the mass transfer rate. Generally, the enhancement factor is defined as the ratio of the absorption flux in the presence of a chemical reaction (chemical absorption) to the absorption flux in the absence of a chemical reaction (physical absorption) for identical mass transfer force. The E of 5 wt% MEA aqueous solution was calculated as 84.4.

Fig. 10 demonstrates the effects of absorbent flow rate on the CO_2 absorption for the SC membrane. When the absorbent flow rate increased from 2 to 9 ml min^{-1}, the CO_2 removal efficiency and CO_2 mass transfer rate increased rapidly from 81.0% to 98.6% and from 3.68 to 4.48 mol m^{-2} h^{-1}, respectively. With a further increase in the absorbent flow rate, the increases of CO_2 removal efficiency and CO_2 mass transfer rate slowed down because nearly all of CO_2 was absorbed at this point. In the case of a liquid flowing through lumen of the hollow fiber, the Sherwood number of liquid phase (Sh_l) can be calculated using Eqs. (4)–(6) [23]:

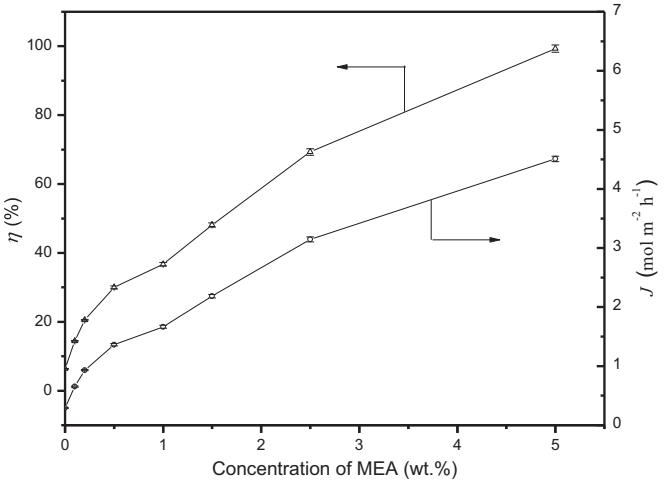

Fig. 9. Effect of MEA concentration on CO_2 absorption for SC membrane (absorbent flow rate of 10 ml min^{-1}; gas flow rate of 50 ml min^{-1}; gas and absorbent temperatures of 293 K; CO_2 concentration in feed gas of 12.5%).

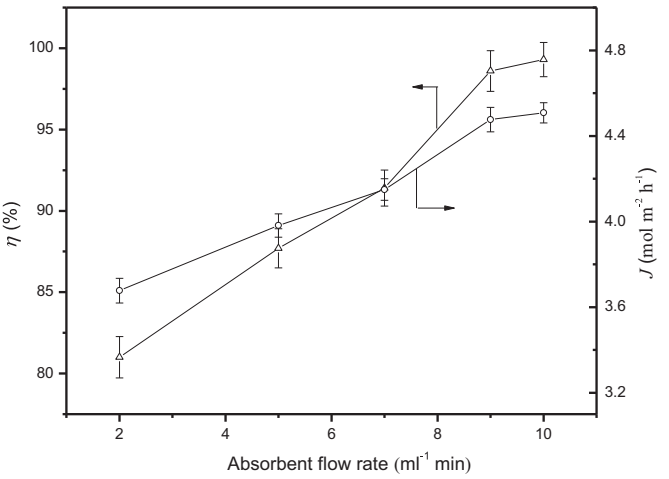

Fig. 10. Effect of absorbent flow rate on CO_2 absorption for SC membrane (gas flow rate of 50 ml min^{-1}; gas and absorbent temperatures of 293 K; absorbent of 5 wt% MEA aqueous solution; CO_2 concentration in feed gas of 12.5%).

$$Sh_l = \frac{k_l d_i}{D_l} = 3.67; \quad Gz < 10 \quad (4)$$

$$Sh_l = 1.62(Gz)^{1/3}; \quad Gz > 20 \quad (5)$$

$$Sh_l = (3.67^3 + 1.62^3 Gz)^{1/3}; \; 10 < Gz < 20 \quad (6)$$

For the SC membrane with absorbent flow rate from 2 to 10 ml min^{-1}, the corresponding Reynolds number ranged from 5.3 to 26.5 and the Graetz number (Gz) was higher than 69.4. An average Sh of 17.0 was obtained for the absorbent flow rate of 10 ml min^{-1} by integrating Eq. (5) over the membrane length. The Gz rises with an increase in flow rate, thus increasing Sh and k_l in accordance with Eqs. (4)–(6). The k_o was enhanced according to Eq. (3), leading to a high CO_2 removal efficiency and CO_2 mass transfer rate.

Given the same volume flow rate ratio of gas to absorbent of 5:1 with the CO_2 concentration of 12.5%, the performances of the SC membrane and PP membrane were compared (see Table 2). For the SC membrane, the resistance corresponding to $1/k_g$ and $1/k_m$ were ignored because the wetting was negligible due to its superhydrophobicity. The theoretical overall mass transfer coefficient (k_o^{theor}) was calculated to be 3.06×10^{-4} m s^{-1}. The experimental overall mass transfer coefficient (k_o^{exp}) was 1.49×10^{-3} m s^{-1} which is 4.87 times k_o^{theor}. It was reported by Fan et al. that the slip of fluid on a superhydrophobic surface under constant heat flux condition makes the temperature profile inside the channel more uniform,

Table 2
Performance comparison between superhydrophobic ceramic membrane and PP membrane.[a]

Module parameters	Module 1	Module 2	Unit
Q_g	50	250	ml min^{-1}
Q_l	10	50	ml min^{-1}
k_o^{theor} at non-wetted mode	3.06×10^{-4}	2.03×10^{-3}	m s^{-1}
k_o^{theor} at wetted mode	–	2.95×10^{-4}	m s^{-1}
k_o^{exp}	1.49×10^{-3}	6.79×10^{-5}	m s^{-1}
J	4.51	0.234	mol m^{-2} h^{-1}
η	99.3	98.8	%
CPA	3742	299	USD m^{-2}
CPC[b]	826	1278	USD h mol^{-1}

[a] Volumetric flow rate ratio of gas to absorbent was 5:1.
[b] $CPC = CPA/J$.

resulting in an increase of heat transfer coefficient or Nusselt number by 1.8 times [35]. Because of the analogy between *Sh* and Nusselt number, in our case, the superhydrophobic surface of the SC membrane most likely intensified the liquid phase mass transfer, giving rise to the higher Sh_l and k_l by experiments than those calculated by Eq. (5) under wall no-slip boundary conditions. This intensification of the liquid phase mass transfer led to the higher k_o^{exp} than k_o^{theor} because the overall mass transfer coefficient depends on the liquid phase mass transfer coefficient for the SC membrane.

For the PP membrane, the membrane resistance depends on the membrane mode of operation (non-wetted, wetted or partially wetted). In the non-wetted (gas-filled pores) and wetted (liquid filled pores) cases, the membrane mass transfer coefficients (k_m) were calculated by Eqs. (7) and (8), respectively. For partially wetted pores, the membrane resistance is a function of the resistance of pores filled with gas, the resistance of pores filled with liquid and the wetting ratio (x, i.e., the ratio of the pore length wetted by liquid to the overall pore length). The k_m in the partially wetted case was calculated by Eq. (9).

$$k_{mg} = \frac{D_{g,eff}\varepsilon_m}{\tau_m l_m} \tag{7}$$

$$k_{ml} = \frac{D_l \varepsilon_m}{\tau_m l_m} \tag{8}$$

$$k_m = \frac{1}{\left(\frac{1-x}{k_{mg}} + \frac{x}{k_{ml}}\right)} \tag{9}$$

As presented in Table 2, for the PP hollow fiber membrane, the k_o^{theor} in the non-wetted mode and wetted mode were 2.03×10^{-3} m s^{-1} and 2.95×10^{-4} m s^{-1}, respectively. However, the corresponding k_o^{exp} was as low as 6.79×10^{-5} m s^{-1}, which is 3.34% and 23.0% of k_o^{theor} in the non-wetted mode and wetted mode, respectively. In other words, even though all of the PP membrane fibers are wetted, the k_o^{theor} is still nearly four times k_o^{exp}. Typically, a hollow fiber membrane module is a bundle of porous hollow fibers packed in parallel alignment into a shell, similar in configuration to a shell and tube heat exchanger. In this structure, the fibers are packed randomly on the shell which gives rise to a non-uniform fiber distribution. So, in our case, there may exist severe fluid channeling and bypassing on the shell side of the module, resulting in a deterioration of the mass transfer process [23]. In addition, in the case of the absorbent flowing through lumen of the thousands of hollow fibers, non-uniform flow distribution most likely occurred, which further lowered the overall mass transfer coefficient. As presented in Table 2, the membrane fabrication cost per effective membrane area (*CPA*) of the SC membrane is 3742 USD m^{-2}, 12.5 times that of the PP hollow fiber membrane. For the the SC membrane, a high CO_2 removal efficiency of 99.3% was achieved with a gas flow rate of 50 ml min^{-1}, which is one fifth of 250 ml min^{-1} for the PP membrane (the CO_2 removal efficiency was 98.8%). The CO_2 mass transfer rate of the SC membrane was 4.51 mol m^{-2} h^{-1}, approximately 19 times that of the PP hollow fiber membrane. Therefore, the SC membrane fabrication cost per absorbed CO_2 flux (*CPC*) was 826 USD h mol^{-1}, 35.4% lower than that of PP hollow fiber membrane.

The effects of operation time on the CO_2 absorption performances of PP membrane and SC membrane were investigated by running the system continuously for 7 days and then drying the membranes at 323 K for 24 h. This procedure is one cycle. As illustrated in Fig. 11, for the fresh PP membrane, the CO_2 removal efficiency and CO_2 mass transfer rate maintained above 90% and 0.22 mol m^{-2} h^{-1}, respectively, within the first 3 days. Then, the CO_2 removal efficiency continuously dropped to 74.2% on the 7th

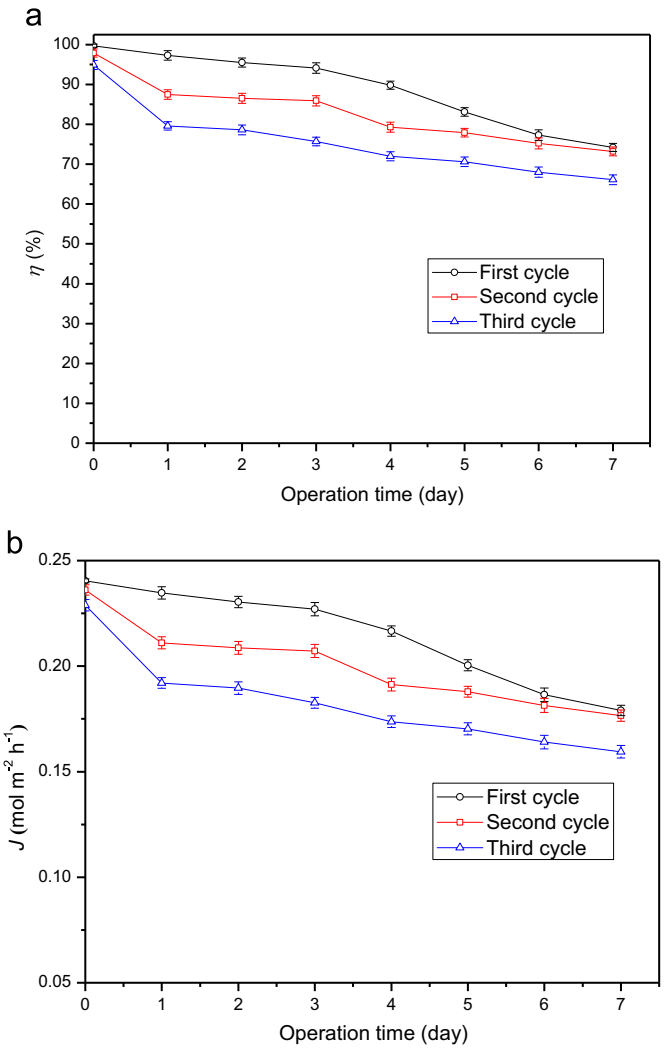

Fig. 11. Effects of operation time on CO_2 absorption for PP hollow fiber membrane: (a) CO_2 removal efficiency; (b) CO_2 mass transfer rate (absorbent flow rate of 50 ml min^{-1}; gas flow rate of 250 ml min^{-1}; gas and absorbent temperatures of 293 K; absorbent of 5 wt% MEA aqueous solution; CO_2 concentration in feed gas of 12.5%).

day. With the increase in the number of cycles, the CO_2 removal efficiency and CO_2 mass transfer rate decreased obviously. The performance of the PP membrane could not be retrieved by drying. This tendency was attributed to the irreversible changes of the PP membrane surface morphologies due to swelling during a long-term exposure of PP fibers to MEA aqueous solution [21]. As demonstrated in Fig. 12, some slit-like membrane pores in the fresh PP fiber sample shrank longitudinally and became elliptical or even circular after three cycles of operation. The pore average equivalent diameter increased with operation time. According to the Laplace–Young equation, the breakthrough pressure decreases with the increase in pore diameter, resulting in more absorbent liquid penetrated into the pores. Therefore, the PP membrane performance deteriorated with operation time according to Eq. (9). For the SC membrane, the CO_2 removal efficiency and CO_2 mass transfer rate continuously decreased with operation time (see Fig. 13), indicating that wetting occurred in a long-term operation despite its superhydrophobicity. The reason for the wetting is unclear and needs further investigation. However, after drying at 323 K, the membrane performance was resumed, suggesting that the grafted fluoroalkylsilane species on the membrane surface were not destroyed during the exposure of membrane to MEA

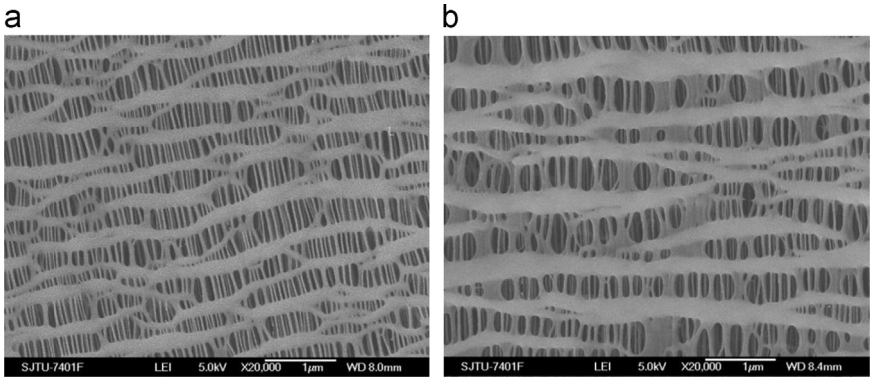

Fig. 12. SEM image of PP membrane surface: (a) fresh; (b) after three cycles operation.

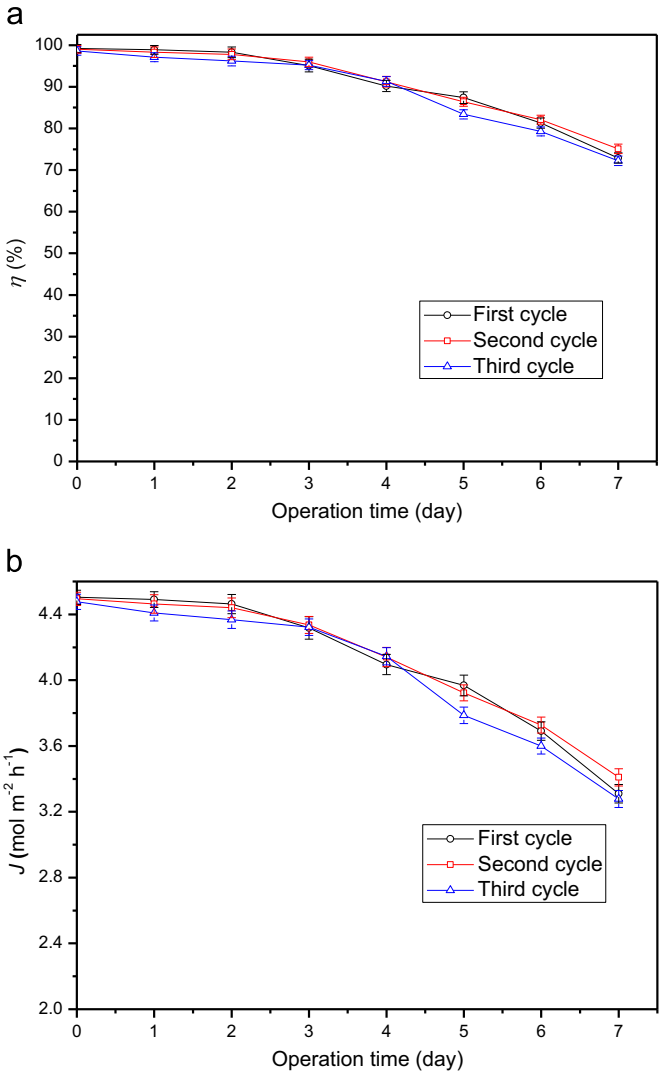

Fig. 13. Effect of operation time on CO_2 absorption for SC membrane: (a) CO_2 removal efficiency; (b) CO_2 mass transfer rate (absorbent flow rate of 10 ml min^{-1}; gas flow rate of 50 ml min^{-1}; gas and absorbent temperatures of 293 K; absorbent of 5 wt% MEA aqueous solution; CO_2 concentration in feed gas of 12.5%).

aqueous solution.

Fig. 14 demonstrated the effects of absorbent temperature on the CO_2 absorption for the SC membrane. When the absorbent temperature increased from 283 to 323 K, the CO_2 removal efficiency and CO_2 mass transfer rate decreased slightly from 99.5% to 94.2% and from 4.52 to 4.28 mol m^{-2} h^{-1}, respectively. The

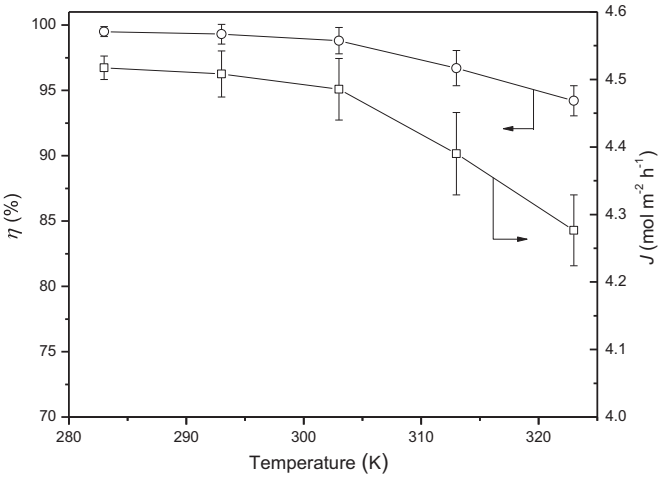

Fig. 14. Effect of absorbent temperature on the CO_2 absorption for SC membrane (gas flow rate of 50 ml min^{-1}; absorbent flow rate of 10 ml min^{-1}; gas temperature of 293 K; absorbent of 5 wt% MEA aqueous solution; CO_2 concentration in feed gas of 12.5%).

unfavorable effects of absorbent temperature are because CO_2 absorption is exothermic.

The effects of feed gas pressure on the CO_2 absorption for the SC membrane are shown in Fig. 15. To prevent the feed gas from bubbling through the membrane pores into the absorbent solution side, the absorbent solution pressure was kept at 0.4 bar, higher than the feed gas pressure (0–0.2 bar). The CO_2 removal efficiency and CO_2 mass transfer rate increased with an increase in gas pressure. For the gas flow rate of 300 ml min^{-1}, the CO_2 removal efficiency and CO_2 mass transfer rate rose from 49.7% to 99.6% and from 13.5 to 27.1 mol m^{-2} h^{-1}, respectively. The CO_2 solubility increases with the rise in feed gas pressure, thus promoting the CO_2 chemical absorption using MEA aqueous solution. For the PP hollow fiber membrane, this promotional effect of high feed gas pressure could not be achieved because the absorbent solution penetrated through the membrane into the feed gas membrane even if the absorbent solution pressure was slightly higher than the feed gas pressure. In our future work, the optimization on the whole CO_2 absorption system will be carried out by weighing the CO_2 absorption and the energy consumption of the feed gas compression.

3.3. *Self-cleaning function*

To test the anti-fouling abilities, the un-grafted ceramic membrane tube, the SC membrane tube and the PP membrane fibers were dipped into carbon powder with an average diameter of

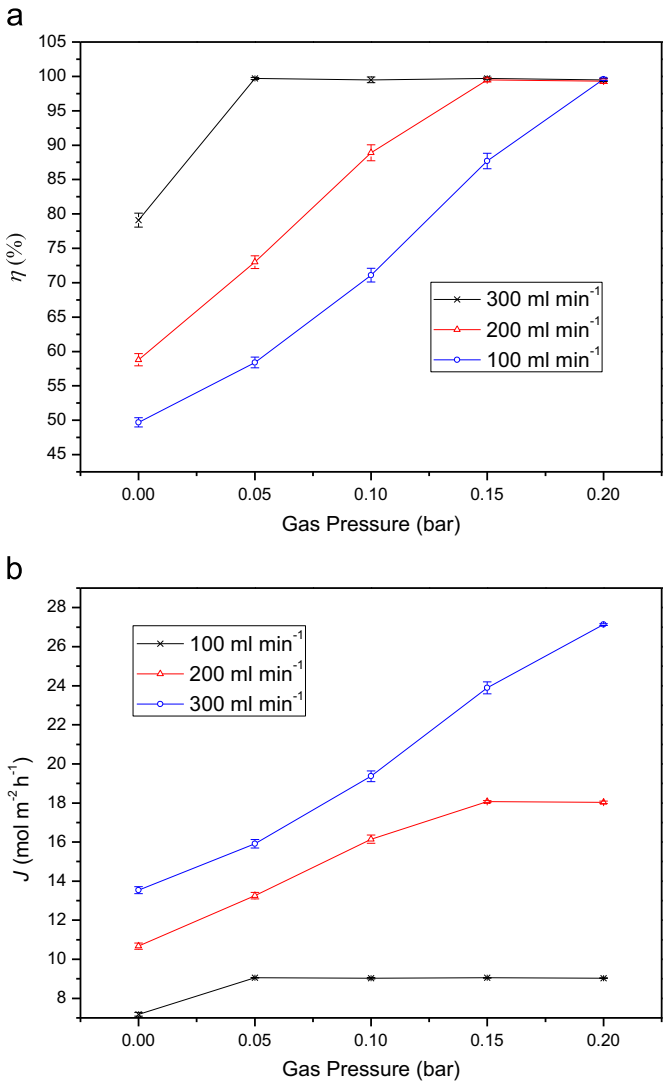

Fig. 15. Effect of feed gas pressure on the CO_2 absorption for SC membrane: (a) CO_2 removal efficiency; (b) CO_2 mass transfer rate (volume flow rate ratio of feed gas to absorbent solution was 5:1; absorbent solution pressure was 0.4 bar; gas and absorbent temperatures of 293 K; absorbent of 5 wt% MEA aqueous solution; CO_2 concentration in feed gas of 12.5%).

5 μm. Then, the SC membrane tube and the PP membrane fibers were washed by water using a syringe with a flow rate of 200 ml min^{-1} in two minutes. As shown in Fig. 16, for the un-grafted ceramic membrane tube and PP membrane fibers, the carbon powder was not effectively removed. In contrast, for the SC membrane tube, most of the carbon powder could be cleaned. Especially, for the membrane layer on the interior surface of the SC membrane tube, almost no left carbon powder was observed after rinsing, revealing a similar self-cleaning function similar to that of a lotus leaf.

To further investigate the anti-fouling of the SC membrane and PP membrane, the two membrane modules were connected to the by-pass of the flue gas main pipeline of Jinjiang Suyuan Thermal Power Plant (Jinjiang City, China). The dusty concentration of the flue gas from coal-fired boiler after the deduster was 30 mg m^{-3}. The flue gas was introduced to the by-pass by a turbine fan and cooled to 323 K. The cooled flue gas flowed into the shell side of the two membrane modules with the gas flow rate of 3 L min^{-1} controlled by a control value. The absorbent did not go through the tube side due to the experimental limitation on site. As shown in Fig. 17(a) and (b), after one-month of operation, no obvious dust

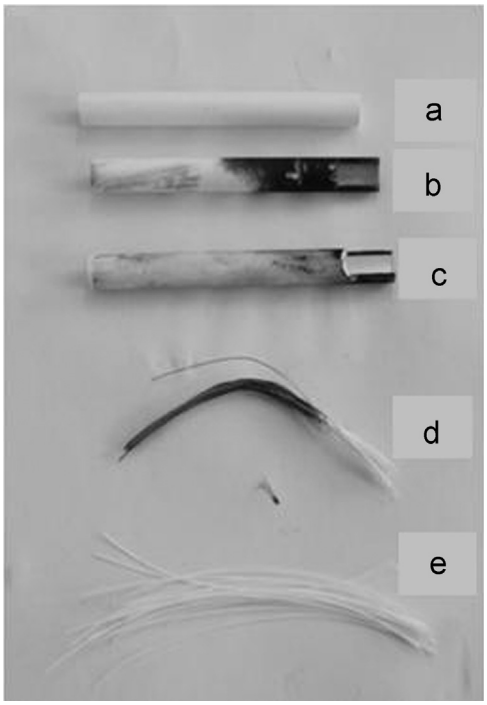

Fig. 16. Images of (a) un-grafted ceramic membrane, (b) un-grafted ceramic membrane dipped into carbon powder and cleaned by water, (c) SC membrane dipped into carbon powder and cleaned by water, (d) PP membrane fibers dipped into carbon powder and cleaned by water, (e) fresh PP membrane fibers.

Fig. 17. Images of (a) fresh SC membrane, (b) SC membrane after one month on site operation, (c) fresh PP hollow fiber membranes and (d) PP membranes after one month on site operation.

was found for the SC membrane. In contrast, many fibers of the PP membranes were fouled by dust in the flue gas (see Fig. 17(c) and (d)). The permeances of the two membranes after one month of operation are illustrated in Fig. 18. For the PP membrane, the permeance decreased by approximately 20% after one month of running (see Fig. 18(a)). Whereas, for the SC membrane, the decrease in permeance was as low as approximately 2% (see Fig. 18 (b)). Therefore, the SC membrane exhibited a better anti-fouling ability than the PP membrane. During the on site experiments, the flue gas was condensed and water was accumulated in the shell side of the membrane module (see Fig. 17(d)). The condensed water could clean the dust on the SC membrane superhydrophobic surface, resulting in a strong anti-fouling ability of the SC membrane.

The SC membrane in our case is not a ceramic hollow fiber membrane because the SC membrane has only one membrane tube with a tube inner diameter of 8 mm which is much higher than that of approximately 1 mm for ceramic hollow fibers [36,37]. However, the grafting procedure with FAS solution can adapt to most of the ceramic hollow fibers. Koonaphapdeelert and Li prepared alumina hollow fiber membranes and modified them to be hydrophobic ones by grafting with 0.01 mol/l of FAS solution [27]. Koonaphapdeelert et al. applied the hydrophobic alumina hollow fiber membranes by FAS with the fiber numbers from 10 to 35 in CO_2 stripping from MEA solution at high temperatures [28]. Zhang et al. modified hydrophilic porous silicon nitride hollow fiber membranes to hydrophobic ones by grafting FAS solution [38]. Therefore, the superhydrophobic ceramic hollow fiber membranes can be prepared by grafting with FAS solution and would exhibit the excellent abilities of anti-wetting and anti-fouling similar to those of the SC membrane in our case.

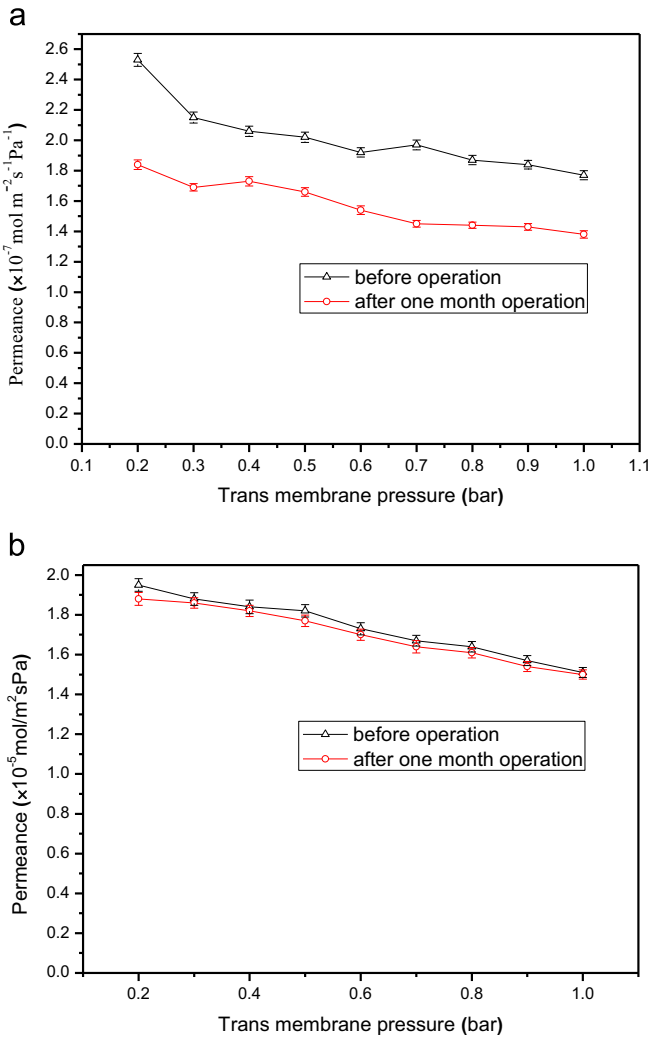

Fig. 18. Effects of suspended particles in flue gas on the permeances of (a) PP membrane and (b) SC membrane (gas flow rate of 3 L min^{-1}; CO_2 concentration of feed gas of 12.5%).

Recent studies have shown the success in the preparation of hollow fiber membranes from ceramic materials such as alumina [36], silicon carbide [37], $La_{0.6}Sr_{0.4}Co_{0.2}Fe_{0.8}O_{3-\alpha}$ [39], etc. On the market, several types of ceramic hollow fiber membranes are available such as InoCep® ceramic hollow fiber membrane (Hyflux®). In addition, the higher ratio of membrane surface area to volume for a SC hollow fiber membrane contactor than the SC membrane contactor in our case can give rise to better performance of the SC hollow fiber membrane contactor in CO_2 capture. The SC hollow fiber membrane contactor has a great potential in the area of CO_2 capture from power plant flue gas.

3.4. *CO_2 capture using SC hollow fiber membrane contactors combined with periodic drying*

To reduce the wetting effect, CO_2 capture using SC hollow fiber membranes combined with drying was proposed. As shown in Fig. 19, two SC hollow fiber membrane contactors (Membrane contactor A and B) were operated alternately to ensure continuous CO_2 removal with high efficiency. Hot flue gas flows into a heat exchanger and is cooled by room temperature air. By opening Valve A and Valve C and closing Valve B and Valve D, the flue gas is introduced into Membrane contactor A and CO_2 was absorbed by the MEA aqueous solution. Meanwhile, Membrane B is dried by the heated air from the heat exchanger. After 5 days running, the CO_2 removal efficiency deceases to approximately 90% according to the results shown in Fig. 13. At this moment, Membrane contactor B was used for CO_2 absorption and Membrane contactor A is dried using heated air by closing Valve A and Valve C and meanwhile opening Valve B and Valve D. In this way, the two SC hollow

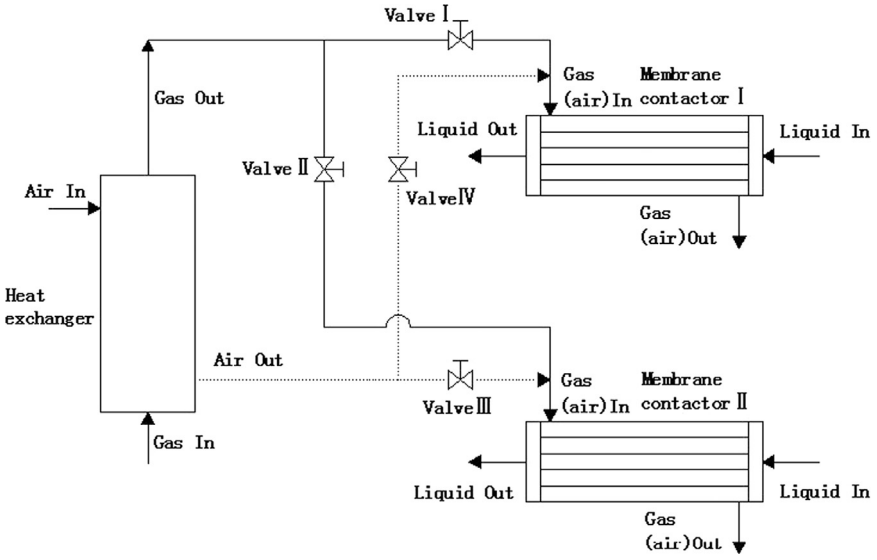

Fig. 19. Schematic diagram of CO_2 capture using SC membrane contactor combined with periodic drying for coal-fired power plant.

fiber membrane contactors can continuously remove above 90% CO_2 from the flue gas of coal-fired power plant. Given the physical and chemical stabilities as well as a strong anti-fouling ability of SC membrane, the proposed CO_2 capture using SC hollow fiber membranes combined with drying should be feasible in real industrial applications.

4. Conclusions

A superhydrophobic ceramic membrane was developed by FAS grafting of an alumina/ZrO_2 tube to handle the problems of wetting and fouling, which is encountered in the membrane gas absorption for CO_2 post-combustion capture of coal-fired power plant. After being grafted with FAS, the ceramic membrane exhibited a contact angle value of 153° and a slightly lower N_2 permeance because the grafted FAS reduces the pore sizes of the membrane slightly. The critical entry pressure for liquid agrees was 5.5 bar for 5 wt% MEA aqueous solution, which agrees well with that calculated value using the Laplace's equation. The *CPC* of the SC membrane was 35.4% lower than that of the PP membrane even though the *CPA* of the SC membrane is 12.5 times that of the PP membrane. For the PP hollow fibers, the k_o^{exp} was as low as 6.79×10^{-5} m s^{-1} which is 3.34% and 23.0% of k_o^{theor} in the non-wetted mode and wetted mode, respectively. This result was attributed to severe fluid channeling and bypassing on the shell side of the module as well as non-uniform flow distribution of absorbent through lumen of thousands of hollow fibers. For the SC membrane, the detrimental effects of wetting could be alleviated by periodic drying to ensure a high CO_2 removal efficiency ($>90\%$), whereas the drying did not work for the PP membrane because the swelling of PP fibers is irreversible. The SC membrane exhibited a better anti-fouling ability than the PP membrane because the superhydrophobic surface featured a self-cleaning function. To ensure continuous CO_2 removal with high efficiency, a method was proposed in which two SC hollow fiber membrane contactors alternately operate, combined with periodic drying. The SC hollow fiber membrane contactor shows great potential in real industrial CO_2 post-combustion capture due to its good anti-wetting and anti-fouling features.

Acknowledgments

This study was financially supported by the China Natural Science Foundation (Contract no. 21176069, 21476073) and the Fundamental Research Funds for the Central Universities (WG1213011).

Nomenclature

C	CO_2 volumetric fraction (%)
CPA	membrane fabrication cost per effective membrane area (USD m^{-2})
CPC	membrane fabrication cost per absorbed CO_2 flux (membrane fabrication cost per absorbed CO_2 flux)
d	diameter of hollow fiber membrane (m)
D	diffusion coefficient (m^2 s^{-1})
E	enhancement factor due to chemical reaction
Gz	Graetz number, $d^2 \cdot \nu/(D \cdot L)$
J	CO_2 mass transfer rate (mol m^2 h^{-1})
k	mass transfer coefficient (m s^{-1})
H	dimensionless Henry's constant
L	length (m)
Q	flow rate (m^3 h^{-1})
S	gas–liquid mass transfer area (m^2)
Sh	Sherwood number
T	temperature (K)
x	pore length wetted by liquid to the overall pore length
ν	velocity (m s^{-1})

Greek letter

ε	membrane porosity
η	CO_2 removal efficiency (%)

Subscripts

g	gas phase
in	inlet
out	outlet
m	membrane or log mean
l	liquid phase
o	outer
i	inner
eff	effective diffusion coefficient of gas in the non-wetted pores
mg	membrane at non-wetted mode
ml	membrane at wetted mode

Superscript

exp	experimental
theor	theoretical

References

[1] S.M. Benson, T. Surles, Carbon dioxide capture and storage: an overview with emphasis on capture and storage in deep geological formations, Proc. IEEE 94 (2006) 1795–1805.
[2] G.Y. Zhao, B. Aziz, N. Hedin, Carbon dioxide adsorption on mesoporous silica surfaces containing amine-like motifs, Appl. Energy 87 (2010) 2907–2913.
[3] L. Zhao, E. Riensche, R. Menzer, L. Blum, D. Stolten, A parametric study of CO_2/N_2 gas separation membrane processes for post-combustion capture, J. Membr. Sci. 325 (2008) 284–294.
[4] M.J. Tuinier, M.V.S. Annaland, G.J. Kramer, J.A.M. Kuipers, Cryogenic CO_2 capture using dynamically operated packed beds, Chem. Eng. Sci. 65 (2010) 114–119.
[5] A. Gabelman, S.T. Hwang, Hollow fiber membrane contactors, J. Membr. Sci. 159 (1999) 61–106.
[6] CO_2 Capture Project (CCP) website, 2005. Available from: http://www.co2capture project.org/index.htm.
[7] M. Mavroudi, S.P. Kaldis, G.P. Sakellaropoulos, Reduction of CO_2 emissions by a membrane contacting process, Fuel 82 (2003) 2153–2159.
[8] S. Yan, M. Fang, W. Zhang, S. Wang, Experimental study on the separation of CO_2 from flue gas using hollow fiber membrane contactors without wetting, Fuel Process. Technol. 88 (2007) 501–511.
[9] A. Bottino, G. Capannelli, A. Comite, R.D. Felice, R. Firpo, CO_2 removal from a gas stream by membrane contactor, Sep. Purif. Technol. 59 (2008) 85–90.
[10] N. Nishikawa, M. Ishibashi, H. Ohata, N. Akutsu, CO_2 removal by hollow fibers gas–liquid contactor, Energy Convers. Manag. 36 (1995) 415–418.
[11] S. Atchariyawut, C. Feng, R. Wang, R. Jiraratananon, D.T. Liang, Effect of membrane structure on mass-transfer in the membrane gas–liquid contacting process using microporous PVDF hollow fibers, J. Membr. Sci. 285 (2006) 272–281.
[12] D. Montigny, P. Tontiwachwuthikul, A. Chakma, Using polypropylene and polytetrafluoroethylene membranes in a membrane contactor for CO_2 absorption, J. Membr. Sci. 277 (2006) 99–107.
[13] A. Mansourizadeh, A.F. Ismail, Effect of additives on the structure and performance of polysulfone hollow fiber membranes for CO_2 absorption, J. Membr. Sci. 348 (2010) 260–267.
[14] K. Li, W.K. Teo, Use of permeation and absorption methods for CO_2 removal in

hollow fiber membrane modules, Sep. Purif. Technol. 13 (1998) 79–88.
[15] R. Wang, D. Li, C. Zhou, Impact of DEA solutions with and without CO_2 loading on porous polypropylene membranes intended for use as contactors, J. Membr. Sci. 229 (2004) 147–157.
[16] A.M. Barbe, P.A. Hogan, R.A. Johnson, Surface morphology changes during initial usage of hydrophobic, microporous polypropylene membranes, J. Membr. Sci. 172 (2000) 149–156.
[17] V.Y. Dindore, D.W. Brilman, P.H. Feron, CO_2 absorption at elevated pressures using a hollow fiber membrane contactor, J. Membr. Sci. 235 (2004) 99–109.
[18] H.Y. Zhang, R. Wang, D.T. Liang, J.H. Tay, Theoretical and experimental studies of membrane wetting in the membrane gas-liquid contacting process for CO_2 absorption, J. Membr. Sci. 203 (2008) 162–170.
[19] P. Keshavarz, J. Fathikalajahi, S. Ayatollahi, Analysis of CO_2 separation and simulation of a partially wetted hollow fiber membrane contactor, J. Hazard. Mater. 152 (2008) 1237–1247.
[20] M. Mavroudi, S.P. Kaldis, G.P. Sakellaropoulos, A study of mass transfer resistance in membrane gas-liquid contacting processes, J. Membr. Sci. 272 (2006) 103–115.
[21] Y.X. Lv, X.H. Yu, S.-T. Tu, J.Y. Yan, E. Dahlquist, Wetting of polypropylene hollow fiber membrane contactors, J. Membr. Sci. 362 (2010) 444–452.
[22] Y.X. Lv, X.H. Yu, J. Jia, S.-T. Tu, J.Y. Yan, E. Dahlquist, Fabrication and characterization of superhydrophobic polypropylene hollow fiber membranes for carbon dioxide absorption, Appl. Energy 90 (2012) 167–174.
[23] A. Mansourizadeh, A.F. Ismail, Hollow fiber gas-liquid membrane contactors for acid gas capture: a review, J. Hazard. Mater. 171 (2009) 38–53.
[24] C. Picard, A. Larbot, J. Sarrazin, P. Janknecht, P. Wilderer, Ceramic membranes for ozonation in wastewater treatment, Ann. Chim. Sci. Matériaux 26 (2001) 13–22.
[25] C. Leger, H.D.L. Lira, R. Paterson, Preparation and properties of surface modified ceramic membranes. Part III. Gas permeation of 5 nm alumina membranes modified by trichloro-octadecylsilane, J. Membr. Sci. 120 (1996) 187–195.
[26] H. Fang, J.F. Gao, H.T. Wang, C.S. Chen, Hydrophobic porous alumina hollow fiber for water desalination via membrane distillation process, J. Membr. Sci. 403 (2012) 41–46.
[27] S. Koonaphapdeelert, K. Li, Preparation and characterization of hydrophobic ceramic hollow fibre membrane, J. Membr. Sci. 291 (2007) 70–76.
[28] S. Koonaphapdeelert, Z.T. Wu, K. Li, Carbon dioxide stripping in ceramic hollow fibre membrane contactors, Chem. Eng. Sci. 64 (2009) 1–8.
[29] E. Jakobs, W.J. Koros, Ceramic membrane characterization via the bubble point technique, J. Membr. Sci. 24 (1997) 149–159.
[30] R.D. Peters, X.M. Yang, T.K. Kim, B.H. Sohn, P.F. Nealey, Using self-assembled monolayers exposed to X-rays to control the wetting behavior of thin films of diblock copolymers, Langmuir 16 (2000) 4625–4631.
[31] M.S. Bourawi, Z. Ding, R. Ma, M. Khayet, A framework for better understanding membrane distillation separation process, J. Membr. Sci. 285 (2006) 4–29.
[32] J. Yang, X.H. Yu, J.Y. Yan, S.-T. Tu, E. Dahlquist, Effects of SO_2 on CO_2 capture using a hollow fiber membrane contactor, Appl. Energy 112 (2013) 755–764.
[33] H.A. Rangwala, Absorption of carbon dioxide into aqueous solutions using hollow fiber membrane contactors, J. Membr. Sci. 112 (1996) 229–240.
[34] R. Wang, H.Y. Zhang, P.H.M. Feron, D.T. Liang, Influence of membrane wetting on CO_2 capture in microporous hollow fiber membrane contactors, Sep. Purif. Technol. 46 (2005) 33–40.
[35] X.X. Fan, Y.H. Zhou, T.Q. Liu, Analysis of laminar heat transfer on superhydrophobic surface with slip velocity, J. Chem. Ind. Eng. 61 (2010) 595–600.
[36] S. Koonaphapdeelert, X. Tan, Z. Wu, K. Li, Solvent distillation by ceramic hollow fibre membrane contactors, J. Membr. Sci. 314 (2008) 58–66.
[37] P. Wit, E.J. Kappert, T. Lohaus, M. Wessling, A. Nijmeijer, N.E. Benes, Highly permeable and mechanically robust silicon carbide hollow fiber membranes, J. Membr. Sci. 475 (2015) 480–487.
[38] J.-W. Zhang, H. Fang, J.-W. Wang, L.-Y. Hao, X. Xu, C.-S. Chen, Preparation and characterization of silicon nitride hollow fiber membranes for seawater desalination, J. Membr. Sci. 450 (2014) 197–206.
[39] R. Wang, B. Meng, X. Meng, X. Tan, J. Sunarso, L. Liu, S. Liu, Highly stable $La_{0.6}Sr_{0.4}Co_{0.2}Fe_{0.8}O_{3-\delta}$ hollow fibre membrane for air separation swept by steam or steam mixture, J. Membr. Sci. 479 (2015) 232–239.